LOCATION OF SEISMICITY WITH A SMALL APERTURE SEISMOMETER ARRAY: IMPLICATIONS FOR SEISMOLOGY WITH AN OCEAN WORLD LANDER. A. G. Marusiak[1], N. C. Schmerr[1], S. H. Bailey[2], D.N. DellaGiustina[2], V.J. Bray[2], P. Dahl[3], E.C. Pettit[4], B. Avenson[5], R. C. Weber[6] [1]University of Maryland College Park, College Park, MD (marusiak@umd.edu), [2] University of Arizona, Lunar and Planetary Laboratory, Tucson AZ, [3]Applied Physics Laboratory University of Washington, Seattle WA, [4] University of Alaska Fairbanks, Fairbank AK, [5]Silicon Audio, Austin TX, [6] NASA Marshall Space Flight Center, Huntsville AL

Introduction: Ocean Worlds, such as Europa, Enceladus, or Titan, have thick icy shells overlying subsurface oceans [1–4]. Due to the potential habitability of Europa's subsurface ocean, the Jovian satellite is a target for a potential lander mission in the late 2020's [5-6]. Part of the Europa lander mission payload is a seismometer that is tasked with locating and identifying sources of seismic activity in the ice shell. Our project, the Seismometer to Investigate Ice and Ocean Structure (SIIOS) is focused on using terrestrial analogs to field test seismic instruments, and to develop techniques for seismic studies on ocean worlds.

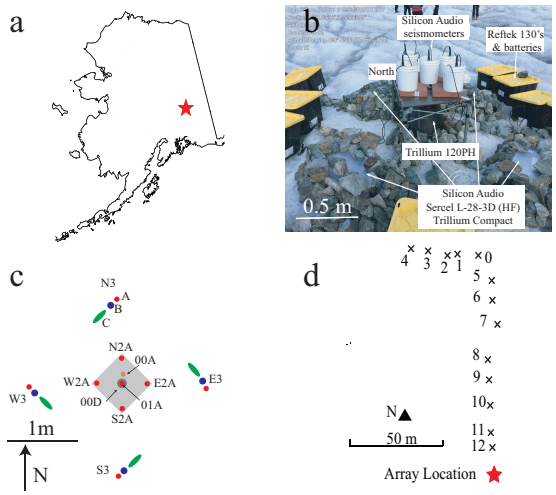

Fig. 1. a) Gulkana Glacier (red star) is located in the Alaskan Range. b) Photo and c) schematic of the SIIOS small aperture seismic array consisting of Silicon Audio (red), Trillium compact (blue), Sercel L28 geophones (green), and a Trillium posthole (black) arranged into a lander-based array (gray) and small aperture array geometry. d) Map of active source location (black x's) relative to the center of the small aperture array (red star).

The SIIOS project deployed seismometers at two terrestrial analog locations: Gulkana Glacier (Fig. 1a) in Alaska and on the Greenland icesheet ~80 km north of Qaanaaq, Greenland. Our analog sites were selected as they have thick ice (40-800 m thick), layers of ice overlying rock and/or water, and an abundance of glacial and icesheet seismicity. In addition, there is seismicity modulated by the diurnal variation in temperature at Gulkana Glacier, although this was absent in Greenland. During each deployment, seismometers were installed in a small aperture seismic array (Fig. 1b,c). The array mimic a lander with seismometers on its legs or placed near the lander (within 1 m) and test the advantage of this system over a single-station seismometer.

Seismic arrays provide improved signal-to-noise ratios, source locations, and resolution of small scale structures [7]. The signal-to-noise ratio of small/weak events is enhanced through linear or phase-weighted stacking. The presence of additional stations enables the use of wavefield coherency to obtain seismic velocities, beam-form [8], and/or perform velocity spectral analysis to recover back azimuth and horizontal slowness.

Seismicity at Gulkana Glacier: SIIOS deployed a small aperture array on Gulkana Glacier from Sept. 8th-23rd, 2017. During that time, the array recorded passive signals, including over a hundred regional events with M_w >2.5. In addition to the passive sources, an active source experiment was conducted to calibrate the sensitivity of the array (Fig. 1d). This experiment allowed us to constrain the local internal structure of the ice [9,10] and to calibrate our source location algorithm against known locations.

The active source signals were generated by striking a 8-kg sledgehammer against a 1.5 cm thick aluminum plate. The experiment was tested at twelve different locations, each with ~ten hammer strikes. The timings of each hammer source were recorded using a GPS Synchronizer with a 1-2 microsecond trigger accuracy. The seismic array recorded data at a 1 kHz sampling rate.

To analyze our data, we first removed the instrument response and filtered to 0.1-250 Hz using a bandpass filter (Fig. 2a). For each location and station, we visually inspected the shots, if necessary we removed shots with bad timings or excess background noise, and then stacked the shots (Fig. 2b).

Location Algorithm: The final stacks were used to pick the arrival of compressional (P) and shear (S) waves (Fig. 2c,d). Five simple one-dimensional velocity models were used to calculate the predicted arrival times of the P and S waves. The models were layered with no low-velocity zones and were based on previous estimates for seismic velocities in ice [11–13]. The algorithm calculated the residual of the predicted versus observed P and S waves using the sum of least squared method [14]. A grid of 400 m x 400 m, centered at the array, was created to perform a source location grid search. The algorithm searched the grid to find where the residuals were minimized to determine the best recovered location. We then computed the chi-squared

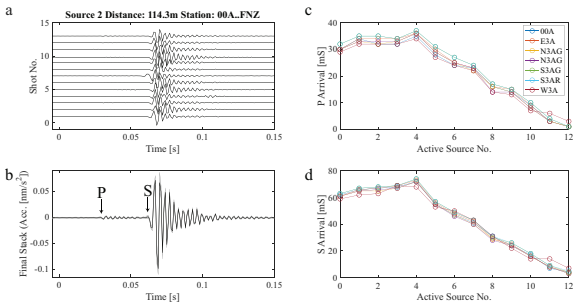

Fig. 2. Individual shots (a) are stacked to enhance the signal-to-noise ratio and pick P and S arrivals (b). The process is repeated for each ground-based, flight-ready instrument (c, d).

cumulative distribution function [14] to determine the most likely locations for each active source (Fig. 3a).

The grid search approach accurately recovers source distance, but additional information is required to constrain the source azimuth. Therefore, we utilized the polarization of the P-wave to determine azimuth via rotation of the horizontals and finding the maximum radial component of motion. At each source-location pair, we created a vector of azimuths ranging from 0-360º in increments of 0.5º. For each azimuth we rotated the horizontal components into the radial and transverse component. Using a time window surrounding the P wave arrival, we searched for large amplitudes in the radial component. The azimuth that produced the greatest amplitude was considered a recovered azimuth.

We repeated this method for each station so we could identify any outliers, and calculate the median along with the 25th and 75th percentiles. (Fig. 3b). This approach was mostly successful except for the two closest events (11 and 12). At short distances the P- and S-wave arrivals are poorly separated in time, making

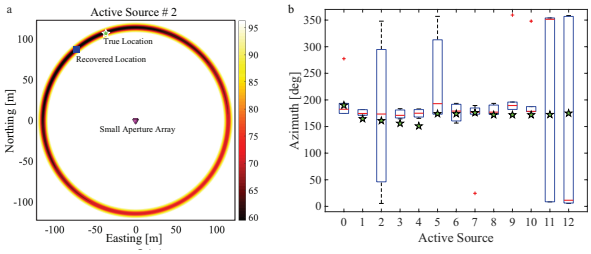

Fig. 3. Recovery of event location using the small aperture array. a) Grid search results to constrain distance using the arrivals of P and S waves. Red/black colorscale indicate the confidence bounds (%) of the location. Blue squares represent the best recovered location. The green stars mark the true azimuth as measured in the field. b) Recovery of azimuth via maximization of radial component energy. Symbols are is in (a). Red lines indicate the median azimuth value, the box encompasses the 25-75th percentiles, dashed lines show values not considered to be outliers, while red crosses show the outliers from one station compared to the rest.

distance determination inaccurate. While the radial maximization of P-wave energy algorithm is able to recover the azimuth for about half of the events, it does not recover the azimuth for all the events.

Future Work: To better recover event azimuths, we will test additional methods, such as using the eigenvectors of the covariance matrix of P arrivals [15–17], polarization of surface waves [18–20], and compressive sensing techniques [8]. These will be jointly inverted with the source location grid search algorithm. We plan to test and improve our location algorithm using the active source experiment conducted at the Greenland field site in addition to regional passive events.

The passive events will also be used to create a catalog of local seismicity. We plan on identifying sources from earthquakes, icequakes, moulins, and rockfalls. The catalog can be used to further quantify the advantages of a small-array over a single-station and detection of nearby small events by an ocean world lander-based array. We can compare not only the number of events the small array detects, but also how well we can locate and identify the sources.

Acknowledgments: This project was funded through NASA PSTAR Grant #80NSSC17K0229 and NASA NESSF Grant # 80NSSC18K1260.

References: [1] Kargel, J. S. *et al. Icarus* **148,** 226–265 (2000).[2] Reynolds, R. T., *et al. Icarus* **56,** 246–254 (1983). [3] Grasset, O., Sotin, C. & Deschamps, F. *Planet. Space Sci.* **48,** 617–636 (2000). [4] Schubert, G., *et al. Icarus* **188,** 345–355 (2007). [5] Hand, K. P. *et al. Report of the Europa Science Definition Team*. (2017). [6] Pappalardo, R. T. *et al. Astrobiology* **13,** 740–773 (2013). [7] Rost, S. & Thomas, C. *Rev. Geophys.* **40,** 1008 (2002). [8] Edelmann, G. F. & Gaumond, C. F. *J. Acoust. Soc. Am.* **130,** EL232-EL237 (2011). [9] Marusiak, A. G. *et al. 49thLPSC* (2018). [10] Marusiak, A. G. *et al. AGU*(2018). [11] Montgomery, L. N. *et al. Front. Earth Sci.* **5,** 10 (2017). [12] Robertson, J. D. & Bentley, C. R. *AGU*, (2013). [13] Shean, D. E. & Marchant, D. R. *J. Glaciol.* **56,** 48–64 (2010). [14] Shearer, P. M. *Introduction to Seismology*. (Cambridge University Press, 2009).[15] Magotra, N., Ahmed, N. & Chael, E. *Trans. Geosci. Remote Sens.* **27,** 15–23 (1989). [16] Frohlich, C. & Pulliam, J. *Phys. Earth Planet. Inter.* **113,** 277–291 (1999). [17] Roberts, R. G., Christoffersson, A. & Cassidy, F. *Geophys. J. Int.* **97,** 471–480 (1989). [18] Panning, M. P. *et al. Icarus* **248,** 230–242 (2015). [19] Bose, M. *et al. Phys. Earth Planet. Inter.* **262,** 48–65 (2017). [20] Khan, A. *et al. Phys. Earth Planet. Inter.* **258,** 28–42 (2016).